Received: 5 August 2022 | Revised: 13 December 2022 | Accepted: 13 December 2022

DOI: 10.1111/nan.12885

ORIGINAL ARTICLE

Neuropathology and Applied Neurobiology
JOURNAL OF THE BRITISH NEUROPATHOLOGICAL SOCIETY

WILEY

m^{6}A mRNA methylation in human brain is disrupted in Lewy body disorders

Braulio Martinez De La Cruz[1] | Chris Gell[2] | Robert Markus[2] | Ian Macdonald[3] | Rupert Fray[4] | Helen Miranda Knight[1]

[1]Division of Cells, Organisms and Molecular Genetics, School of Life Sciences, University of Nottingham, Nottingham, UK

[2]School of Life Sciences Imaging Facility, University of Nottingham, Nottingham, UK

[3]Division of Physiology, Pharmacology and Neuroscience, School of Life Sciences, University of Nottingham, Nottingham, UK

[4]Division of Plant Sciences, School of Biosciences, University of Nottingham, Nottingham, UK

Correspondence
Helen Miranda Knight, School of Life Sciences, Queen's Medical Centre, University of Nottingham, Nottingham NG7 2UH, UK.
Email: helen.knight@nottingham.ac.uk

Present address
Braulio Martinez De La Cruz, LMCB, University College London, London, UK.

Funding information
The work was funded by Nottingham University, UK. Braulio Martinez De La Cruz was supported by a CONACYT PhD scholarship.

Abstract

Aims: N^6-methyladenosine modification of RNA (m^{6}A) regulates translational control, which may influence neuronal dysfunction underlying neurodegenerative diseases.

Methods: Using microscopy and a machine learning approach, we performed cellular profiling of m^{6}A-RNA abundance and YTHDF1/YTHDF3 m^{6}A reader expression within four regions of the human brain from non-affected individuals and individuals with Parkinson's disease, dementia with Lewy bodies or mild cognitive impairment (MCI).

Results: In non-diseased tissue, we found that m^{6}A-modified RNAs showed cell-type and sub-compartment-specific variation. YTHDF1 and YTHDF3 showed opposing expression patterns in the cerebellum and the frontal and cingulate cortices. Machine learning quantitative image analysis revealed that m^{6}A-modified transcripts were significantly altered in localisation and abundance in disease tissue with significant decreases in m^{6}A-RNAs in Parkinson's disease, and significant increases in m^{6}A-RNA abundance in dementia with Lewy bodies. MCI tissue showed variability across regions but similar to DLB; in brain areas with an overall significant increase in m^{6}A-RNAs, modified RNAs within dendritic processes were reduced. Using mass spectrometry proteomic datasets to corroborate our findings, we found significant changes in YTHDF3 and m^{6}A anti-reader protein abundance in Alzheimer's disease (AD) and asymptomatic AD/MCI tissue and correlation with cognitive resilience.

Conclusions: These results provide evidence for disrupted m^{6}A regulation in Lewy body diseases and a plausible mechanism through which RNA processing could contribute to the formation of Lewy bodies and other dementia-associated pathological aggregates. The findings suggest that manipulation of epitranscriptomic processes influencing translational control may lead to new therapeutic approaches for neurodegenerative diseases.

KEYWORDS
dementia with Lewy bodies, epitranscriptomics, Lewy body disease, m^{6}A, mild cognitive impairment, Parkinson's disease, RNA methylation

INTRODUCTION

N^6-methyladenosine (m^6A) and the cap-adjacent N^6,2′-O-dimethyladenosine (m^6A_m) are highly abundant and reversible mRNA modifications [1, 2]. m^6A modification is regulated by effector proteins termed writer, eraser and reader proteins. RNA binding proteins belonging to the reader category recognise specific chemical modifications and direct binding events [3, 4]. The best-characterised m^6A readers belong to the YTH domain family, which consists of YTHDF1, YTHDF2, YTHDF3, YTHDC and YTHDC2. The YTHDF1–3 proteins have similar sequence identity and binding affinities toward preferred RNA motifs [5, 6], and recent studies support dosage-dependent redundancy in their function to regulate m^6A-dependent mRNA stability and translation [7–9]. However, context-specific factors are proposed to determine each of their unique roles in moderating cellular protein turnover required for specialised physiological processes [10]. In addition to YTH domain reader proteins that interact with m^6A RNA modified sites, several proteins have been identified as preferentially interacting with unmodified m^6A RNA binding sequences, that is, they are repelled by 'm^6A' RNA modifications and are hence referred to as m^6A anti-readers [11, 12].

Synaptic plasticity is widely accepted as the main neural basis of learning and memory and when disrupted gives rise to neurological disease. Evidence now exists that m^6A-methylated transcripts and effector protein machinery are involved in synaptic function, as well as glial cell plasticity and neuronal development [13–16]. For instance, m^6A-modified RNAs, the YTHDF proteins and the ALKBH5 eraser protein are located at actively translating synapses and involved in early- and late-stage synaptic plasticity [14], and disrupting writer, reader and eraser effector protein function, for example, METTL3, YTHDF1, and FTO, gives rise to changes in plasticity, behaviour and cognition [17–19]. Furthermore, m^6A methylome mapping of mouse forebrain synaptosomes and human parahippocampus brain tissue also indicates that synaptic and neuronal transcripts and RNAs associated with increased risk for cognitive diseases are commonly m^6A modified [14, 20].

Dementia with Lewy bodies (DLB) and Parkinson's disease (PD) are common progressive neurodegenerative diseases [21]. At the prodromal stages of DLB, as with other dementia-related disorders such as Alzheimer's disease (AD), mild cognitive impairment (MCI) is a common feature, although only individuals with non-amnestic MCI progress to develop DLB [22–24]. Both DLB and PD are classified as α-synucleinopathies as the neuropathological hallmarks are large abnormal α-synuclein (α-syn) aggregates within the cytoplasm of neurons known as Lewy bodies and associated dendritic structures termed Lewy neurites [23–26]. However, early PD pathology is characterised by the loss of dopaminergic neurotransmission in the medulla, substantia nigra and cerebellum [27–29], whereas in DLB, abnormal deposits of α-syn at synaptic sites accumulate within the neocortex and limbic system regions [30, 31]. In both diseases, large α-syn aggregates are initially regionally localised, but at later stages, pathology progressively spreads to other areas of the brain [32]. Although the underlying mechanisms that drive neuropathological spreading are currently still under debate, one hypothesis is that specific molecular factors may act as a 'seed' for the formation of neurotoxic aggregates in other regions [33]. Furthermore, with the recent discovery that the YTHDF reader proteins are intrinsically disordered proteins [9, 34] that can promote the formation of highly condensed macromolecular aggregates, this leaves open the possibility that m^6A RNA modification within neurons may influence abnormal protein aggregation.

To better understand the importance of m^6A RNA methylation in human brain physiology and Lewy body diseases, we performed cellular profiling of m^6A RNA abundance and YTHDF1 and YTHDF3 m^6A reader protein expression within cell populations of the cerebellum, frontal and cingulate gyrus cortices and the hippocampus in aged individuals with no disease and from individuals with a diagnosis of PD, DLB or MCI. m^6A profiling revealed that modified transcripts and YTHDF readers were found to be significantly altered in the localisation and abundance within PD, DLB and MCI brain tissue. YTHDF3 and specific anti-reader proteins were also found to change in abundance in AD brain tissue. The results provide evidence for m^6A regulation disruption in Lewy body diseases and other degenerative neurocognitive conditions, and a plausible mechanism influencing translational control, which drives the formation of toxic protein aggregates.

Key points

- m^6A RNA modification influences the fate of RNAs and has been associated with the formation of highly condensed macromolecular aggregates.
- The distribution of m^6A-RNAs in specific cell populations in human brain tissue and evidence for changes in Lewy body disease has not yet been investigated.
- m^6A-modified RNAs were found consistently more abundant in dementia with Lewy bodies tissue and significantly reduced or misplaced in brain tissue from individuals with Parkinson's disease.
- The findings of disrupted localisation and abundance of m^6A RNAs in Lewy body diseases are consistent with evidence for alterations in the control of RNA translation contributing to the formation of protein aggregate neurotoxic structures.

MATERIALS AND METHODS

Brain tissue

Non-affected, healthy brain tissue samples were obtained from the Nottingham Health Science Biobank (Biobank reference ID

ACP0000101). Individuals were at an advanced age at the time of death (mean 85 years, ranging from 63 to 99 years old), but the brains were classified as non-disease-affected by a neuropathologist. MCI, PD and DLB brain tissue samples and associated clinical and neuropathological data were supplied by the Parkinson's UK Brain Bank, funded by Parkinson's UK, a charity registered in England and Wales (258197) and in Scotland (SC037554). These samples had a mean age of 82.5 years and ranged from 63 to 104 years old. Ethical permission to collect and use human samples was previously granted to both tissue banks by the relevant multicentre research ethical committees (Parkinson's UK Brain Bank approval Ref. No. 08/MRE09/31+5). Demographic details and neuropathology at autopsy per tissue sample are presented in Table S1. Tissue from four different brain regions was examined: the cerebellum, cingulate gyrus, middle frontal gyrus and hippocampus. These areas were chosen to enable comparison of regions of the brain that undergo pathological changes in MCI, DLB and PD at early or later stages of the disease. Three sections from non-affected aged control, PD, DLB and MCI tissue per region were examined. No differences in age or sex were evident between affected and non-affected samples. Post-mortem interval data were available for only a subset of PD and DLB brains (Table S1).

Immunohistochemistry

Sections were dewaxed and rehydrated by immersion in xylene and ethanol. Antigen retrieval was conducted by immersing sections in sodium citrate. Protein and endogenous peroxidases were blocked by incubation with horse serum and by immersing sections in 3% hydrogen peroxide. Endogenous avidin, biotin and biotin receptors were blocked by incubating sections in Avidin D followed by Biotin (Avidin/Biotin Blocking Kit, Vector Labs). Primary antibodies were diluted in 0.2% Triton X-100, and sections were incubated overnight. A universal secondary antibody was incubated with slides for 1 h before incubation with Vectastain ABC Reagent (Vectastain Elite ABC Kit, Vector Labs, USA) for 30 min. Tissue sections were finally incubated with ImmPACT DAB substrate, counterstained in haematoxylin and Scott's tap water, and dehydrated. Positive (GFAP immunoreactivity) and negative controls were included for each experiment.

Antibodies and bright field microscopy

The following primary antibodies and dilutions were used: mouse anti-m^{6}A (Merck Millipore, MABE 1006, clone 17-3-4-1) 1:50, mouse anti-YTHDF3 (Santa Cruz Biotech, sc-377119) 1:200, rabbit anti-m^{6}A (Abcam, ab190886) 1:250, rabbit anti-YTHDF1 (Abcam, ab99080) 1:100, mouse anti-NeuN (Merck Millipore, MAB377) 1:100 and rabbit anti-GFAP (ThermoFisher, RM-2125-S) 1:50. The mouse anti-m^{6}A (Merck Millipore, MABE 1006), consistent with other anti-m^{6}A antibodies, does not show immunoreactivity in the nucleus of cells in cell cultures or FFPE tissue [14]. Images of immunostained tissue were captured using the Micro Manager open-source microscope controller software [35] on an Axioplan microscope (Carl Zeiss, Germany). All images were captured using a 20× air objective (NA = 0.5) with an exposure time of 35 ms. A blank image was captured and used to white balance all other experimental images using a macro created to apply the same degree of colour intensity change to all images.

Image analysis of IHC using machine learning

Quantitative localisation was performed blind using the ilastik open-source image classification and segmentation software (www.ilastik.org) [36, 37]. Ilastik uses machine learning algorithms to automatically, but under supervision, quantify features in an image. All feature selection algorithms were set at a threshold of $\sigma = 1.0$. Two labels were used in the training modules; one to identify and train for brown DAB staining and one to teach the exclusion of blue haematoxylin staining. After training, experimental images were batch processed, and the probability maps generated were exported as .tiff files and used in FIJI as masks. A macro was run in FIJI to calculate and record mean pixel intensity values. A pipeline for this analysis is presented in Figure S1. One-way ANOVAs and Dunnett's multiple comparison tests were undertaken to assess statistical significance. Statistical tests and the generation of graphs were performed using GraphPad Prism.

Data analysis of effector proteins using tandem mass tag mass spectrometry (TMT-MS) quantitative proteomic datasets

Tandem mass tag mass spectrometry (TMT-MS) data from the dorsal lateral prefrontal cortex (DLPFC) published by Johnson et al. [38] and Yu et al. [39] were examined for changes in YTHDF1 and YTHDF3 protein abundance and 18 human cytoplasmic m^{6}A anti-readers reported by Edupuganti et al. [12]. The anti-reader proteins examined were METTL16, THUMD1, DUS3L, SRSF9, SRSF6, SRSF5, SRSF4, SRSF1, ZC3HAV1, LSM12, DNAJC13, ATXN2L, POLD1, NUFIP2, CAPRIN1, USP10, G3BP1 and G3BP2. The Johnson et al.'s dataset performed TMT-MS using AD, Asymptomatic AD (AsymAD) and unaffected control brain tissue from the Religious Orders Study and Memory and Aging Project (ROSMAP, $n = 84$ control, 148 AsymAD and 108 AD) and the Banner Sun Health Research Institute (Banner, $n = 26$ control, 58 AsymAD and 92 AD) [38]. Asymptomatic AD samples in this dataset are similar in phenotype to MCI. In addition to quantifying protein levels, individual protein abundance was correlated with performance in the mini-mental state examination (MMSE); Braak staging; CERAD scores; alpha-synuclein (SNCA) and TARDBP [TDP-43]; and amyloid beta 6–28 protein measures. In the Yu et al. study, cognitive resilience was quantified using cognitive and clinical evaluations [39]. Further details of methods and statistical analyses are provided by [38, 39].

RESULTS

m^{6}A-modified RNA distribution within neuronal cells in the aged human brain

Using an antibody specific for m^{6}A-modified RNAs, we characterised m^{6}A-RNA distribution and abundance in non-diseased aged human brain tissue. We observed m^{6}A-modified transcripts throughout all cytoplasmic regions, including axons and dendrites, of neuronal and glial cells, but an m^{6}A signal was absent from the nucleus. M^{6}A-modified RNAs were observed within the three main regions of the cerebellum, the outermost molecular layer (ML), the Purkinje cell layer (PL) and the granular cell layer (GL), although there was some clear variation in the presence and abundance of modified RNAs between cells. Medium to high abundance of m^{6}A-modified RNA was observed around the nucleus of inhibitory interneurons in the ML, within the cytoplasm of the granular layer cells and large Purkinje cells and in putative Bergmann glia cells. Strong m^{6}A abundance was observed in the processes of the Purkinje cells, which extended into the molecular layer (Figure S2).

We next examined the abundance of modified RNAs within the cingulate gyrus (CG), a part of the limbic system reported to be one of the first areas in DLB to accumulate α-synuclein aggregates at synapses as well as large cytoplasmic Lewy bodies. Within the six cortical layer structure (Figure 1, column 1), glial cells and processes within Layer I and granular cells within Layers II and IV showed a high abundance of m^{6}A RNAs. Within Layer III pyramidal cells, m^{6}A immunoreactivity was found to be darker near the nucleus and lighter within the cytoplasm along neuronal processes indicating fewer modified RNAs. However, the large pyramidal cells of Layer V were darkly immunostained throughout the cytoplasm. Finally, Layer VI contained a mixture of immunoreactive cell types showing varying degrees of m^{6}A abundance. Consistent with the CG, observations of the frontal cortex (FC), also a cortical region, revealed similar m^{6}A-modified RNA abundance (Figure S3). However, a decrease in modified m^{6}A RNAs was observed within the cell body and processes of pyramidal cells within Layer V.

m^{6}A modified RNA profiles were also characterised within the hippocampal formation, a region in which neuropathological changes associated with dementias contribute to cognitive decline. Within the dentate gyrus granular cell layer, a site where adult neurogenesis occurs, widespread m^{6}A immunoreactivity was observed (Figure 2). In the dentate gyrus hilar region, m^{6}A-modified RNAs were observed in large pyramidal cells and along extended processes of mossy cell and CA4 field neurons. Putative small inhibitory basket cells within this region appeared to have few modified RNAs. In the Cornu Ammonis (CA) fields outside of the dentate gyrus, individual neurons within the CA4 and CA3/2 were all similarly stained. The hippocampus CA1 field displayed the most variance in m^{6}A immunostaining with some cells showing low overall immunoreactivity while others were darkly stained in the cytoplasm. The location of m^{6}A-RNAs also varied between the cytoplasm and axons in CA1 cells.

m^{6}A-readers YTHDF1 and YTHDF3 expression in human brain

We next characterised YTHDF1 and YTHDF3 expression across the same four brain regions. YTHDF1 was found to be expressed in all layers of the cerebellum with cell type-specific variation. Expression of YTHDF1 within the Purkinje cells was especially high in the cytoplasm including neuronal/dendritic processes but these cells had low or no YTHDF3 expression (Figures S4 and S5). Similarly, YTHDF1 was also highly expressed in the GL whereas few cells in the GL were immuno-positive for YTHDF3. The abundance of YTHDF1 and YTHDF3 varied in the CG and FC cortices and contrasted with the pattern observed in the cerebellum. YTHDF1 abundance in both cortical regions was generally low across cell populations. An exception was pyramidal neurons within layer III that had high cytoplasmic expression and layers V-VI where YTHDF1 was consistently located in the cytoplasm opposite to the axon, that is, showed a polarised pattern. Conversely, YTHDF3 abundance was high in all layers of CG and layers I–IV of FC (Figure S6). However, within FC the large pyramidal cells of layer V had very low immunoreactivity and interestingly, YTHDF3 staining was also not observed in the neuronal processes of pyramidal cells. The lack of expression of YTHDF1 and YTHDF3 readers within processes of layer V cortical pyramidal cells deviates from our previous observation of high m^{6}A-modified mRNA in these same pyramidal cells.

Within the hippocampus, low levels of cytoplasmic YTHDF1 expression were observed within the dentate gyrus granular cells and large neurons within the hilar, while in the CA4 primary neurons, strong m^{6}A abundance was evident but restricted to neuronal soma (Figure S7). Within the CA3/CA2 and CA1 fields, YTHDF1 was highly abundant in small cytoplasmic clusters, whereas in CA1 pyramidal neurons YTHDF1 was also evident in axons. YTHDF3 expression was observed in all sub-regions of the hippocampus (Figure S8). In the CA fields, pyramidal cells displayed strong YTHDF3 immunoreactivity as a distinctive ring pattern in soma, which might reflect high YTHDF3 expression in the endoplasmic reticulum. In contrast to YTHDF1 in the CA1, YTHDF3 was absent from neuronal processes. These results suggest that YTHDF1 and YTHDF3 are co-expressed within pyramidal neurons but they also differentially localise within cell sub-compartments.

Quantitative image analysis of m^{6}A-modified RNAs and YTHDF1/YTHDF3 abundance in PD, DLB and MCI brain tissue

Cerebellum

To examine whether m^{6}A processes are disrupted in Lewy body diseases, we examined brain tissue from individuals with PD, DLB and MCI and performed unbiased machine learning quantification of m^{6}A staining intensities. In the cerebellum, there was a significant increase in m^{6}A abundance across the entire cerebellum in PD, (Ctrl 120.8

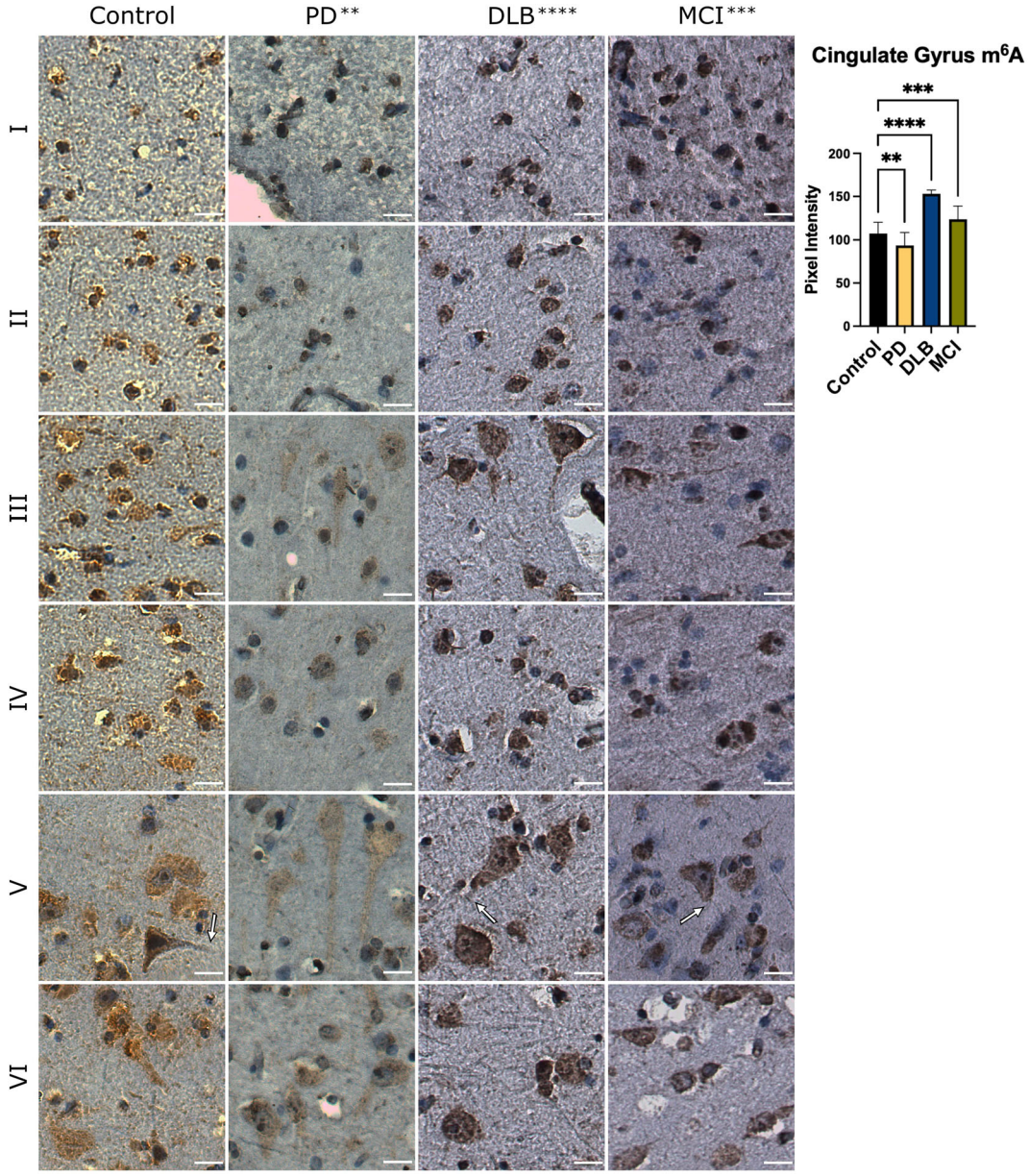

FIGURE 1 m^{6}A-modified transcripts in non-affected and diseased tissue within the cingulate gyrus in tissue. m^{6}A-modified transcripts were found abundant in cells of all six cortical layers, I–VI (rows 1–6). The location and abundance of m^{6}A-modified transcripts were found to significantly differ in disease tissue with an overall decrease in m^{6}A-modified RNAs in PD and an overall increase in DLB and MCI tissue. White arrows indicate changes in subcellular localisation of m^{6}A-modified transcripts between control and disease samples. DLB, dementia with Lewy bodies; GL, granular layer. MCI, mild cognitive impairment; ML, molecular layer; PD, Parkinson's disease; PL, Purkinje layer. $^{**}p \leq 0.01$, $^{***}p \leq 0.001$, $^{****}p \leq 0.0001$. Scale bar = 20 μm.

± 21.31, PD 149.5 ± 24.14, $p \leq 0.005$), DLB (149.8 ± 26.05; $p \leq 0.0005$) and MCI tissue samples (MCI 154.8 ± 27.00; $p \leq 0.0001$; Figure S2 and Table 1). However, the large Purkinje cells in all disease tissue had reduced or no m^{6}A expression as compared with unaffected control tissue (Figure S2, yellow arrows). Counter to m^{6}A abundance, we observed a significant reduction in YTHDF1 expression in PD cerebellum tissue (Ctrl 113.7 ± 25.42, PD 95.02 ± 20.82; $p \leq 0.005$), with no YTHDF1 expression in Purkinje cells or cells within the molecular layer (Figure S4, column 2). Like PD tissue, MCI tissue showed an overall reduced YTHDF1 expression (MCI 99.88 ± 23.87; $p \leq 0.05$). This contrasted significantly with YTHDF1 expression in DLB tissue which was found to be of comparative abundance and distribution as non-affected control tissue (DLB 108.2 ± 23.77; $p > 0.65$, Figure S4, column 3). YTHDF3 expression was found to be significantly increased in the cerebellum of all disease tissues compared with control tissue (Ctrl 136.9 ± 25.52, PD 160.1 ± 20.7, $p \leq 0.0005$; DLB 158.7 ± 20.17, $p \leq 0.0005$; MCI 158.9 ± 23.33, $p \leq 0.001$; Figure S5). However, Purkinje cells in PD samples had either no or very low

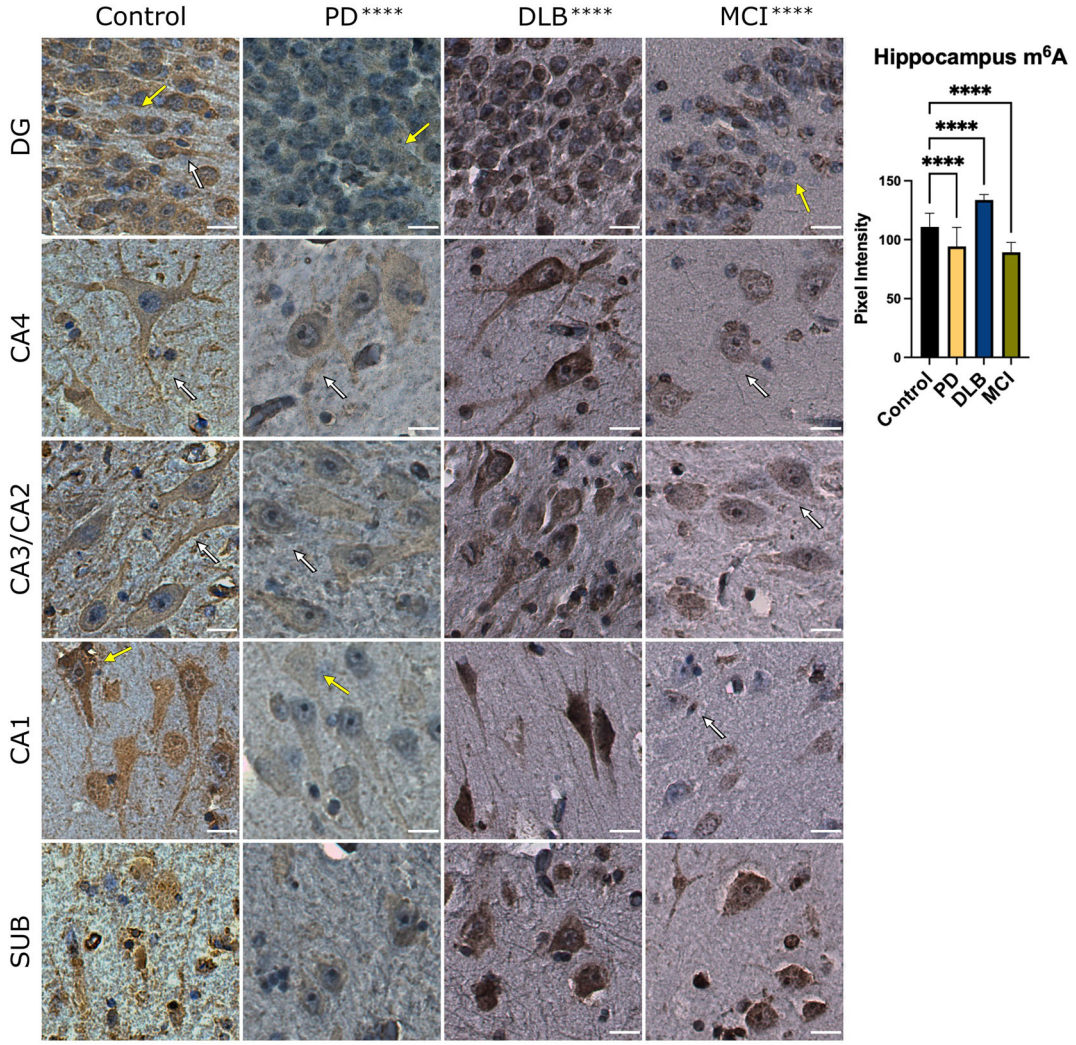

FIGURE 2 m^{6}A-modified spatial profiling in the hippocampus in healthy and diseased brain tissue. m^{6}A-modified transcripts were found to be highly prevalent in granular cells of the dentate gyrus and pyramidal neuron cytoplasm and processes. Arrows point to sites where differential abundance was observed between diseases. Yellow arrows indicate changes in abundance between control and disease samples, and white arrows indicate changes in subcellular localisation of m^{6}A-modified transcripts between control and disease samples. CA, cornu ammonis; DG, dentate gyrus; DLB, dementia with Lewy bodies; MCI, mild cognitive impairment, PD, Parkinson's disease; SUB, subiculum. ****$p \leq 0.0001$. Scale bar = 20 μm.

YTHDF3 immunoreactivity and in DLB tissue YTHDF3 was observed in the cytoplasm but not proximal neuronal processes. Finally, MCI tissue showed some Purkinje cells had high, medium, or low YTHDF3 expression in the cytoplasm and proximal neuronal processes.

Frontal cortex and cingulate gyrus

Cingulate gyrus tissue showed an overall increased m^{6}A abundance in DLB and MCI (Ctrl 107.5 ± 12.66, DLB 153.0 ± 4.43, $p \leq 0.0001$; MCI 123.5 ± 15.43; $p \leq 0.0005$; Figure 1). However, in Layer V of the CG in DLB and MCI tissue, a notable decrease in the number of m^{6}A-stained pyramidal neuron processes was observed despite an overall increase in the expression of m^{6}A modifications in these cells. Furthermore, pyramidal neurons in Layer VI of CG and FC tissue in MCI individuals indicated a polarised distribution with m^{6}A abundance localised to the cytoplasmic region opposite the cell's axon, a pattern which was also evident for YTHDF1 expression in this cortical layer in non-affected tissue (Figures 1 and S3). DLB tissue also showed a similar decrease in pyramidal neuron processes immunoreactivity but an overall increase in m^{6}A methylation levels (Figure S3, column 3) in both cytoplasm and processes of cells within the FC (Ctrl 116.8 ± 6.14, DLB 136.3 ± 9.13, $p \leq 0.001$).

Compared with control tissue, CG and FC cortical regions in PD tissue revealed a large decrease in m^{6}A modification abundance (CG Ctrl 107.5 ± 12.66, PD 93.57 ± 15.09, $p \leq 0.005$; FC Ctrl 116.8 ± 6.14, PD 109.1 ± 6.71, $p \leq 0.05$) but notably, modified RNAs in pyramidal processes remained apparent and numerous and the spatial distribution and localisation of m^{6}A abundance within cells was generally unchanged (Figure 1, column 2, Figure S3, column 2). MCI tissue

TABLE 1 Mean quantitative abundance of m^{6}A-modified RNAs and YTHDF1 and YTHDF3 reader proteins across brain regions and in healthy, PD, DLB and MCI tissue.

Brain region		Control abundance	Disease	Disease abundance	*p* value
Cerebellum	m^{6}A	120.8 ± 21.3	PD	149.5 ± 24.1**	<0.005
			DLB	149.8 ± 26.1***	<0.0005
			MCI	154.8 ± 27.0****	<0.0001
	YTHDF1	113.7 ± 25.4	PD	95.0 ± 20.8**	0.005
			DLB	108.2 ± 23.8	0.65
			MCI	99.9 ± 23.9*	<0.05
	YTHDF3	136.9 ± 25.5	PD	160.1 ± 20.7***	<0.0005
			DLB	158.7 ± 20.2***	<0.0005
			MCI	158.9 ± 23.3***	<0.001
Frontal cortex	m^{6}A	116.8 ± 6.1	PD	109.1 ± 6.7*	<0.05
			DLB	136.3 ± 9.1****	<0.0001
			MCI	102.3 ± 17.0****	<0.0001
	YTHDF1	118.7 ± 6.4	PD	116.5 ± 5.7	0.49
			DLB	118.1 ± 10.3*	0.98
			MCI	120.6 ± 6.2	0.69
	YTHDF3	128.7 ± 9.6	PD	123.4 ± 7.6*	<0.05
			DLB	133.7 ± 4.2*	<0.05
			MCI	131.8 ± 6.0	0.21
Cingulate gyrus	m^{6}A	107.5 ± 12.7	PD	93.6 ± 15.1**	<0.005
			DLB	153.0 ± 4.4****	<0.0001
			MCI	123.5 ± 15.4***	<0.0005
	YTHDF1	135.9 ± 10.5	PD	124.0 ± 18.8**	<0.005
			DLB	135.4 ± 5.2	0.99
			MCI	141.6 ± 9.8	0.24
	YTHDF3	120.5 ± 11.2	PD	106.4 ± 11.0****	<0.0001
			DLB	136.4 ± 6.8****	<0.0001
			MCI	111.2 ± 8.3**	<0.005
Hippocampus	m^{6}A	110.8 ± 11.7	PD	94.0 ± 16.3****	<0.0001
			DLB	133.7 ± 4.6****	<0.0001
			MCI	89.2 ± 8.5****	<0.0001
	YTHDF1	122.2 ± 16.5	PD	141.4 ± 14.5****	<0.0001
			DLB	138.6 ± 9.3****	<0.0001
			MCI	109.4 ± 8.5***	<0.0005
	YTHDF3	118.2 ± 10.8	PD	145.4 ± 6.6****	<0.0001
			DLB	137.1 ± 6.5****	<0.0001
			MCI	121.4 ± 4.3	0.12

Note: Mean abundance or protein expression in affected and control tissue and *p* values for differences in abundance are presented for the cerebellum, frontal and cingulate cortices and the hippocampal regions. *p* values presented are corrected for multiple comparisons.
Abbreviations: DLB, dementia with Lewy bodies; MCI, mild cognitive impairment; PD, Parkinson's disease.
*$p \leq 0.05$.
**$p \leq 0.01$.
***$p \leq 0.001$.
****$p \leq 0.0001$.

in the frontal cortex also showed an overall decrease in m^{6}A abundance (FC Ctrl 116.8 ± 6.14, MCI 102.3 ± 16.97, $p \leq 0.0001$), a pattern opposite to the increased m^{6}A abundance in the CG. Of interest, layer V showed a clear decrease in immunoreactivity in neuronal processes, and unlike PD tissue, also showed decreased m^{6}A modified RNAs in large pyramidal layer V neuronal processes.

YTHDF1 expression in the CG and FC PD tissue was globally reduced although this change in abundance was significant only for the CG (CG Ctrl 135.9 ± 10.54, PD 124.0 ± 18.82, $p \leq 0.005$; FC Ctrl 118.7 ± 6.37, PD 116.5 ± 5.7, $p > 0.49$). Decreased expression was most notable in Layer III and Layers V-VI. For DLB and MCI tissue, no overall quantitative differences were identified for YTHDF1 expression in either the CG or FC (CG Ctrl 135.9 ± 10.54, DLB 135.4 ± 5.22, $p > 0.99$; MCI 141.6 ± 9.76; $p > 0.24$; FC Ctrl 118.7 ± 6.37, DLB 118.1 ± 10.34, $p > 0.98$; MCI 120.6 ± 6.2, $p > 0.69$). However, in MCI tissue Layers III and V of CG, YTHDF1 expression was not observed in processes.

YTHDF3 expression was found reduced in PD samples within the CG and FC (CG Ctrl 120.5 ± 11.24, PD 106.4 ± 11.02, $p \leq 0.0001$; FC Ctrl 128.7 ± 9.62, PD 123.4 ± 7.63, $p < 0.05$) and this decrease was evident across all cortical layers (Figure S6). An overall decrease in YTHDF3 expression in MCI tissue was found in the CG (CG Ctrl 120.5 ± 11.24, MCI 111.2 ± 8.26, $p \leq 0.005$) but no significant differences in expression for the FC (FC Ctrl 128.7 ± 9.62, MCI 131.8 ± 6.01, $p > 0.21$). In contrast, YTHDF3 expression in DLB CG and FC tissue saw a global increase (CG Ctrl 120.5 ± 11.24, DLB 136.4 ± 6.8, $p \leq 0.0001$; FC Ctrl 128.7 ± 9.62, DLB 133.7 ± 4.2, $p < 0.05$).

Hippocampus

Consistent with other regions of the brain, PD-affected hippocampal tissue had significantly reduced overall m^{6}A-modified RNAs (Ctrl 110.8 ± 11.65, PD 94.02 ± 16.27, $p \leq 0.0001$). The intensity of staining in dentate gyrus neurons was lower and processes did not show m^{6}A immunoreactivity (Figure 2). Likewise, we did not observe modified transcripts in the neuronal processes of CA4 and CA3/CA2 neurons but in the CA1 field, although m^{6}A abundance was reduced, some processes were m^{6}A-positive (Figure 2, rows 2–4). In contrast to PD, but consistent with all three other regions, DLB samples showed a significant increase in m^{6}A abundance, (Ctrl 110.8 ± 11.65, DLB 133.7 ± 4.59, $p \leq 0.0001$). However, patterns of subcellular localisation including within processes did not appear different to unaffected control tissue. MCI-affected hippocampal tissue showed the largest reduction in m^{6}A expression (Ctrl 110.8 ± 11.65, MCI 89.16 ± 8.45, $p \leq 0.0001$), and compared with controls tissue, there was a lack of modified transcripts in dentate gyrus cells including granular cells as well as within neuronal processes in all CA fields (Figure 2, column 4, rows 1–4).

Global YTHDF1 expression was increased in PD and DLB samples within the hippocampus (Ctrl 122.2 ± 16.46, PD 141.4 ± 14.48, $p \leq 0.0001$; DLB 138.6 ± 9.32, $p \leq 0.0001$), where highly increased cytoplasmic and axonal expression was observed in the CA fields (Figure S7). However, the expression of YTHDF1 was reduced in MCI samples (Ctrl 122.2 ± 16.46, MCI 109.2 ± 8.45, $p \leq 0.0005$). A global increase of YTHDF3 immunoreactivity was also evident in PD (Ctrl 118.2 ± 10.79, PD 145.4 ± 6.63, $p \leq 0.0001$) and DLB (Ctrl 118.2 ± 10.79, DLB 137.1 ± 6.55, $p \leq 0.001$) (Figure S8) and in particular, in PD tissue within the dentate gyrus and CA3/CA2 cells. Expression of YTHDF3 did not appear to differ in MCI from the control tissue (Ctrl 118.2 ± 10.79, MCI 121.4 ± 4.31, $p = 0.12$). These significant changes in m^{6}A methylation abundance and reader expression patterns suggest that m^{6}A methylation is a key mechanism underlying RNA processing, which is dysregulated in the hippocampus of individuals with Lewy body disease or MCI.

Factors which influence changes in YTHDF protein sublocalisation within cells or abundance across cell populations are not well characterised but may include feedback systems involving m^{6}A autoregulation of effector reader proteins, reader Lnc RNAs, for example, *YTHDF3-AS1*, or m^{6}A anti-reader proteins [14]. In an attempt to first provide corroborating evidence supporting our findings that the YTHDF1 and YTHDF3 m^{6}A reader proteins change in abundance in neurodegenerative disease brain tissue, we examined tandem mass tag mass spectrometry (TMT-MS) proteomic datasets which assessed protein abundance in the prefrontal cortex and quantified differences between individuals with AD, asymptomatic AD and healthy control individuals [38] or protein associations with cognitive resilience [39]. We found that YTHDF3 protein abundance was significantly lower in the prefrontal cortex in individuals with AD (post hoc FDR corrected p value, AD vs control $p = 0.003$; AD vs AsymAD $p = 0.006$) and that YTHDF3 protein abundance showed a significant positive correlation with high cognitive performance in the MMSE ($p = 0.03$), as well as positive correlations with α-syn [SCNA] ($p = 0.009$) and TARDBP ($p = 1.92 \times 10^{-10}$) protein levels. In contrast, a negative correlation between YTHDF3 protein levels and CERAD pathology score ($p = 0.046$) was observed. YTHDF3 protein abundance was also reported to be significantly positively associated with cognitive resilience which is consistent with lower YTHDF3 abundance in cognitively impaired AD individuals (Table S2). YTHDF1 indicated no differences in expression in the prefrontal cortex across AD, AsymAD or control groupings and no correlations with pathological or cognitive measures.

We hypothesised that if significant changes to m^{6}A reader protein localisation and abundance occur across neurodegenerative disease tissues, anti-reader proteins, which may influence m^{6}A RNA binding protein complexes and could be part of an autoregulatory feedback mechanism, would also show changes with disease. On analysing the protein abundance of the 18 cytoplasmic anti-readers, we discovered that 9 of the 18 anti-reader proteins showed significant differences in abundance between AD/AsymAD and control tissue (Table S2). These significant differences included both increases and decreases in protein expression in AD suggesting context-specific factors influence effector protein localisation and function. Furthermore, one anti-reader protein, ATXN2L, like YTHDF3, also showed a significant association with cognitive resilience. These findings support that reader and anti-reader protein abundance change across neurodegenerative diseases and that the direction of change in m^{6}A effector machinery, like changes in m^{6}A modified RNA, are different depending on the disease, for example, AD, PD or DLB.

DISCUSSION

The processes leading to neurodegeneration in brain tissue will involve disruption to normal cellular turnover of RNAs and proteins in subcellular compartments. m^{6}A modification regulates translation, degradation and stability across most RNA species known. However, whether, how and where disruption to m^{6}A modified-RNA contributes to Lewy body pathology, is still unknown. In healthy brain tissue, we observed m^{6}A-RNAs in most cytoplasmic regions including in both neuronal and glial cells. High abundance was observed in dendritic processes of specific neuronal cell populations, for example, cortical pyramidal layers III, V and VI, CA regions of the hippocampus and granular cells of the dentate gyrus, but, found sparse or inconsistently abundant within processes of pyramidal cells of the subiculum and Purkinje cells of the cerebellum. Of note, and consistent with reports that m^{6}A modification governs cell fate determination [40], self-renewal of mouse embryonic stem cells [41] and prolongs embryonic cortical neurogenesis [16], we observed in non-disease tissue high abundance of modified RNAs within potential stems cells in the SGZ of the hippocampus, as well as in the large mossy fibre cells of the dentate gyrus. Changes in m^{6}A-modified RNA abundance in these 'neurogenic' cell populations were evident in PD, DLB and MCI tissue but showed contrasting patterns of change across the Lewy body diseases. For example, in PD and MCI, m^{6}A-RNAs were reduced in dentate gyrus neurons and were no longer located in the processes, whereas in DLB, there was a significant increase in m^{6}A-RNAs, but no evident change in subcellular localisation. Whether demethylation by ALKBH5 controls modified RNA abundance within sub-cellular compartments and thus influences the development and proliferation of SGZ cells, as evident in developing mouse cerebellar cells [42], remains to be determined.

m^{6}A abundance was found to be significantly altered in diseased tissue in all brain regions examined but showed consistent opposing patterns across neurodegenerative disorders (Figure 3). In PD tissue, the abundance of m^{6}A-modified RNAs was significantly decreased across all regions except for the cerebellum where modified RNAs were significantly more abundant than in the healthy tissue. However, within the cerebellum, Purkinje cells showed no, or reduced, m^{6}A-RNAs and YTHDF3 abundance within the cytosol. This is of interest because Purkinje cell loss or depletion of Purkinje cell processes has been repeatedly reported in Parkinsonism [31, 43], and hence, our findings support that RNA processing mechanisms may be contributing to such Parkinson's disease cerebellar dysfunction. The significantly decreased abundance of modified RNA in PD in the cytosol of cells found throughout the hippocampus and in both cortical regions could have a significant influence on cytoplasmic protein turnover and protein subcellular distribution and aggregation, affecting known molecular neuropathological processes. As yet, the mechanisms that may be determining why modified RNAs are significantly reduced are not known but could involve disruption to m^{6}A RNAs transport out of the nucleus into the cytoplasm or could increase demethylation processing occurring at localised cytoplasmic sites.

DLB tissue showed a significant increase in both modified RNAs and YTHDF3 expression across all regions although in some areas such as the hippocampus, the pattern of m^{6}A-RNA subcellular localisation did not differ from the unaffected tissue. Futhermore, MCI tissue showed variability with both significant increases and decreases in m^{6}A abundance across brain areas and similar to DLB, in brain areas where there was an overall increase in m^{6}A-RNAs, modified RNAs within dendritic processes were found to be reduced. Mass spectrometry proteomic data of prefrontal tissue also substantiated that m^{6}A effector machinery is altered in AD and extended the findings to include anti-reader proteins. Together, these findings suggest that there may be independent molecular switches that govern changes in modified RNA abundance within the cell compartments and functional subcellular structures and that differ between neurodegenerative

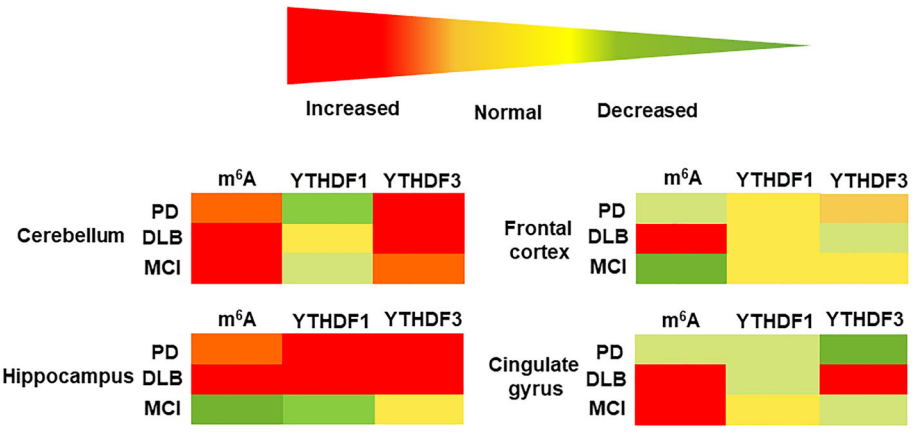

FIGURE 3 Heat chart of changes in abundance of m^{6}A-modified RNAs and YTHDF1 and YTHDF3 reader proteins across brain regions and in healthy aged, PD, DLB and MCI tissue. Increased red, normal yellow, and decreased green for m^{6}A-modified RNAs abundance and YTHDF1 and YTHDF3 expression across regions and within disease categories. DLB tissue was found to have consistently increased abundance of m^{6}A-modified RNAs across all brain tissue regions as well general increases in YTHDF1 and YTHDF3 expression compared with healthy control tissue. PD tissue, in contrast, showed significantly reduced m^{6}A-modified RNAs in three brain regions and no consistent pattern of changes in YTHDF reader protein expression. DLB, dementia with Lewy bodies; MCI, mild cognitive impairment; PD, Parkinson's disease.

diseases and, potentially, stage of disease pathology. Future m^{6}A mRNA mapping studies using base resolution techniques such as miCLiP-seq [44] and brain tissue from clinical populations are needed to determine which transcripts change their modification profiles in disease.

The study is not without limitations. First, the cellular profiling of m^{6}A-RNAs was conducted with relatively few samples per disease group, and a possible difference between amnestic and non-amnestic MCI cases was not explored. Moreover, the approach adopted cannot distinguish whether significant increases or decreases in m^{6}A-modified RNA abundance are owing to changes in the number of modified mRNAs or a change in the number of modifications along mRNAs, that is, an increase or decrease in multi-modified transcripts. However, evidence providing further support for our findings that m^{6}A processes are disrupted in neurodegenerative disease is beginning to emerge. First, RNA-binding motif protein 3 (RMB3), an RNA-binding protein involved in cellular stress response, which is known to increase global protein synthesis rates including in dendrites [45, 46], was recently predicted to bind to m^{6}A modified sites, that is, act as an alternative m^{6}A effector reader protein [47]. RBM3 knockdown has been found to exacerbate synaptic loss in mouse prion and AD models of disease, whereas enhanced expression of RBM3 restores the capacity for synapse repair after cooling [48]. Second, HNRNPA2B1, an m^{6}A writer that influences splicing [49], associates with oligomeric tau and m^{6}A-RNAs, and in late-stage AD temporal cortical tissue, global HNRNPA2B1, tau and m^{6}A-RNAs are all found increased in abundance [50]. Indeed, the cytoplasmic distribution of m^{6}A immunoreactivity in severe AD cases was found much broader than Tau or HNRNPA2B1, suggesting that changes in the m^{6}A modification process begin earlier, and may be independent of HNRNPA2B1 or tau pathology [50]. Third, α-syn RNA is m^{6}A modified in brain tissue as are several proteins which interact with α-syn including β-synuclein and γ-synuclein [13, 14, 51]. Furthermore, α-syn undergoes extensive protein phosphorylation in synuclein aggregates in DLB and PD tissue and is commonly found ubiquitinated in Lewy bodies [52, 53]. Proteins involved in both these post-translational modification processes have to be found significantly enriched for m^{6}A-modified transcripts in brain tissue [14]. With the uncovering role of multi-modified-m^{6}A mRNAs in promoting the formation of highly condensed membraneless macromolecular aggregates [9, 34, 54, 55], our study provides a novel avenue to explore mechanisms which drive the formation of neurotoxic Lewy aggregates. Together, our findings provide support that manipulation of common epitranscriptomic processes influencing translational control may lead to new therapies preventing synaptic failure and neuronal pathology across the spectrum of neurodegenerative diseases.

AUTHOR CONTRIBUTIONS

Helen Miranda Knight, Rupert George Fray, Ian A Macdonald and Braulio Martinez De La Cruz designed the study. Braulio Martinez De La Cruz performed the microscopy experiments and Braulio Martinez De La Cruz, Chris Gell and Robert Markus contributed to the image data analysis. Helen Miranda Knight performed mass spectrometry data mining. Helen Miranda Knight and Braulio Martinez De La Cruz wrote the manuscript. The first draft of the manuscript was written by Helen Miranda Knight, and all authors commented on previous versions of the manuscript. All authors read and approved the final manuscript.

ACKNOWLEDGEMENTS

The project was funded by Nottingham University, UK. B Martinez De La Cruz was supported by a CONACYT PhD scholarship. We thank the Nottingham Health Science Biobank and the Parkinson's UK Brain Bank for providing brain samples.

CONFLICT OF INTEREST STATEMENT

The authors have no competing interests to declare that are relevant to the content of this article.

DATA AVAILABILITY STATEMENT

All data analysed during this study are included in this published article and its supplementary information files. The macro generated for image analysis is available upon request.

ETHICS STATEMENT

Ethical permission to collect and use human samples was previously granted to the Nottingham Health Science Biobank and Parkinson's UK Brain tissue banks by the relevant multicentre research ethical committees (Parkinson's UK Brain Bank approval Ref. No. 08/MRE09/31+5).

REFERENCES

1. Dominissini D, Moshitch-Moshkovitz S, Schwartz S, et al. Topology of the human and mouse m6A RNA methylomes revealed by m6A-seq. *Nature*. 2012;485(7397):201-206. doi:10.1038/nature11112
2. Meyer KD, Saletore Y, Zumbo P, Elemento O, Mason CE, Jaffrey SR. Comprehensive analysis of mRNA methylation reveals enrichment in 3′ UTRs and near stop codons. *Cell*. 2012;149(7):1635-1646. doi:10.1016/j.cell.2012.05.003
3. Huang H, Weng H, Sun W, et al. Recognition of RNA N^6-methyladenosine by IGF2BP proteins enhances mRNA stability and translation. *Nat Cell Biol*. 2018;20(3):285-295. doi:10.1038/s41556-018-0045-z
4. Liu N, Dai Q, Zheng G, He C, Parisien M, Pan T. N(6)-methyladenosine-dependent RNA structural switches regulate RNA-protein interactions. *Nature*. 2015;518(7540):560-564. doi:10.1038/nature14234
5. Li A, Chen YS, Ping XL, et al. Cytoplasmic m^{6}a reader YTHDF3 promotes mRNA translation. *Cell Res*. 2017;27(3):444-447. doi:10.1038/cr.2017.10
6. Li Y, Bedi RK, Moroz-Omori EV, Caflisch A. Structural and dynamic insights into redundant function of YTHDF proteins. *J Chem Inf Model*. 2020;60(12):5932-5935. doi:10.1021/acs.jcim.0c01029
7. Kontur C, Jeong M, Cifuentes D, Giraldez AJ. Ythdf m^{6}a readers function redundantly during zebrafish development. *Cell Rep*. 2020;33(13):108598. doi:10.1016/j.celrep.2020.108598
8. Luo S, Tong L. Molecular basis for the recognition of methylated adenines in RNA by the eukaryotic YTH domain. *Proc Natl Acad Sci U S a*. 2014;111(38):13834-13839. doi:10.1073/pnas.1412742111

9. Ries RJ, Zaccara S, Klein P, et al. m^{6}a enhances the phase separation potential of mRNA. *Nature*. 2019;571(7765):424-428. doi:10.1038/s41586-019-1374-1
10. Lasman L, Krupalnik V, Viukov S, et al. Context-dependent functional compensation between Ythdf m^{6}a reader proteins. *Genes Dev*. 2020;34(19–20):1373-1391. doi:10.1101/gad.340695.120
11. Arguello AE, DeLiberto AN, Kleiner RE. RNA chemical proteomics reveals the N^6-methyladenosine (m^{6}A)-regulated protein–RNA Interactome. *J am Chem Soc*. 2017;139(48):17249-17252. doi:10.1021/jacs.7b09213
12. Edupuganti RR, Geiger S, Lindeboom RGH, et al. N^6-methyladenosine (m^{6}a) recruits and repels proteins to regulate mRNA homeostasis. *Nat Struct Mol Biol*. 2017;24(10):870-878. doi:10.1038/nsmb.3462
13. Breydo L, Wu JW, Uversky VN. Alpha-synuclein misfolding and Parkinson's disease. *Biochim Biophys Acta*. 2012;1822(2):261-285. doi:10.1016/j.bbadis.2011.10.002
14. Martinez De La Cruz B, Markus R, Malla S, et al. Modifying the m^{6}a brain methylome by ALKBH5-mediated demethylation: a new contender for synaptic tagging. *Mol Psychiatry*. 2021;26(12):7141-7153. doi:10.1038/s41380-021-01282-z
15. Xu H, Dzhashiashvili Y, Shah A, et al. m^{6}a mRNA methylation is essential for oligodendrocyte maturation and CNS myelination. *Neuron*. 2020;105(2):293-309 e5. doi:10.1016/j.neuron.2019.12.013
16. Yoon KJ, Ringeling FR, Vissers C, et al. Temporal control of mammalian cortical neurogenesis by m^{6}a methylation. *Cell*. 2017;171(4):877-89 e17. doi:10.1016/j.cell.2017.09.003
17. Hess ME, Hess S, Meyer KD, et al. The fat mass and obesity associated gene (Fto) regulates activity of the dopaminergic midbrain circuitry. *Nat Neurosci*. 2013;16(8):1042-1048. doi:10.1038/nn.3449
18. Shi H, Zhang X, Weng YL, et al. m^{6}a facilitates hippocampus-dependent learning and memory through YTHDF1. *Nature*. 2018;563(7730):249-253. doi:10.1038/s41586-018-0666-1
19. Zhang Z, Wang M, Xie D, et al. METTL3-mediated N^6-methyladenosine mRNA modification enhances long-term memory consolidation. *Cell Res*. 2018;28(11):1050-1061. doi:10.1038/s41422-018-0092-9
20. Merkurjev D, Hong WT, Iida K, et al. Synaptic N^6-methyladenosine (m^{6}a) epitranscriptome reveals functional partitioning of localized transcripts. *Nat Neurosci*. 2018;21(7):1004-1014. doi:10.1038/s41593-018-0173-6
21. McKeith IG, Boeve BF, Dickson DW, et al. Diagnosis and management of dementia with Lewy bodies: fourth consensus report of the DLB consortium. *Neurology*. 2017;89(1):88-100. doi:10.1212/WNL.0000000000004058
22. Aarsland D. Cognitive impairment in Parkinson's disease and dementia with Lewy bodies. *Parkinsonism Relat Disord*. 2016;22(Suppl 1):S144-S148. doi:10.1016/j.parkreldis.2015.09.034
23. Aarsland D, Bronnick K, Fladby T. Mild cognitive impairment in Parkinson's disease. *Curr Neurol Neurosci Rep*. 2011;11(4):371-378. doi:10.1007/s11910-011-0203-1
24. Ferman TJ, Smith GE, Kantarci K, et al. Nonamnestic mild cognitive impairment progresses to dementia with Lewy bodies. *Neurology*. 2013;81(23):2032-2038. doi:10.1212/01.wnl.0000436942.55281.47
25. Goedert M, Spillantini MG, Del Tredici K, Braak H. 100 years of Lewy pathology. *Nat Rev Neurol*. 2013;9(1):13-24. doi:10.1038/nrneurol.2012.242
26. Spillantini MG, Schmidt ML, Lee VM, Trojanowski JQ, Jakes R, Goedert M. Alpha-synuclein in Lewy bodies. *Nature*. 1997;388(6645):839-840. doi:10.1038/42166
27. Damier P, Hirsch EC, Agid Y, Graybiel AM. The substantia nigra of the human brain. II. Patterns of loss of dopamine-containing neurons in Parkinson's disease. *Brain*. 1999;122(Pt 8):1437-1448. doi:10.1093/brain/122.8.1437
28. Tsuboi Y, Uchikado H, Dickson DW. Neuropathology of Parkinson's disease dementia and dementia with Lewy bodies with reference to striatal pathology. *Parkinsonism Relat Disord*. 2007;13(Suppl 3):S221-S224. doi:10.1016/S1353-8020(08)70005-1
29. Wu T, Hallett M. The cerebellum in Parkinson's disease. *Brain*. 2013;136(Pt 3):696-709. doi:10.1093/brain/aws360
30. Colom-Cadena M, Pegueroles J, Herrmann AG, et al. Synaptic phosphorylated alpha-synuclein in dementia with Lewy bodies. *Brain*. 2017;140(12):3204-3214. doi:10.1093/brain/awx275
31. Schulz-Schaeffer WJ. The synaptic pathology of alpha-synuclein aggregation in dementia with Lewy bodies, Parkinson's disease and Parkinson's disease dementia. *Acta Neuropathol*. 2010;120(2):131-143. doi:10.1007/s00401-010-0711-0
32. Beach TG, Adler CH, Lue L, et al. Unified staging system for Lewy body disorders: correlation with nigrostriatal degeneration, cognitive impairment and motor dysfunction. *Acta Neuropathol*. 2009;117(6):613-634. doi:10.1007/s00401-009-0538-8
33. Luk KC, Song C, O'Brien P, et al. Exogenous alpha-synuclein fibrils seed the formation of Lewy body-like intracellular inclusions in cultured cells. *Proc Natl Acad Sci U S a*. 2009;106(47):20051-20056. doi:10.1073/pnas.0908005106
34. Gao Y, Pei G, Li D, et al. Multivalent m^{6}a motifs promote phase separation of YTHDF proteins. *Cell Res*. 2019;29(9):767-769. doi:10.1038/s41422-019-0210-3
35. Edelstein A, Amodaj N, Hoover K, Vale R, Stuurman N. Computer control of microscopes using microManager. *Curr Protoc Mol Biol*. 2010;92(1):Unit14.20. doi:10.1002/0471142727.mb1420s92
36. Berg S, Kutra D, Kroeger T, et al. Ilastik: interactive machine learning for (bio)image analysis. *Nat Methods*. 2019;16(12):1226-1232. doi:10.1038/s41592-019-0582-9
37. Kan A. Machine learning applications in cell image analysis. *Immunol Cell Biol*. 2017;95(6):525-530. doi:10.1038/icb.2017.16
38. Johnson ECB, Carter EK, Dammer EB, et al. Large-scale deep multi-layer analysis of Alzheimer's disease brain reveals strong proteomic disease-related changes not observed at the RNA level. *Nat Neurosci*. 2022;25(2):213-225. doi:10.1038/s41593-021-00999-y
39. Yu L, Tasaki S, Schneider JA, et al. Cortical proteins associated with cognitive resilience in community-dwelling older persons. *JAMA Psych*. 2020;77(11):1172-1180. doi:10.1001/jamapsychiatry.2020.1807
40. Agarwala SD, Blitzblau HG, Hochwagen A, Fink GR. RNA methylation by the MIS complex regulates a cell fate decision in yeast. *PLoS Genet*. 2012;8(6):e1002732. doi:10.1371/journal.pgen.1002732
41. Wang Y, Li Y, Toth JI, Petroski MD, Zhang Z, Zhao JC. N^6-methyladenosine modification destabilizes developmental regulators in embryonic stem cells. *Nat Cell Biol*. 2014;16(2):191-198. doi:10.1038/ncb2902
42. Ma C, Chang M, Lv H, et al. RNA m^{6}a methylation participates in regulation of postnatal development of the mouse cerebellum. *Genome Biol*. 2018;19(1):68. doi:10.1186/s13059-018-1435-z
43. Rolland AS, Herrero MT, Garcia-Martinez V, Ruberg M, Hirsch EC, Francois C. Metabolic activity of cerebellar and basal ganglia-thalamic neurons is reduced in parkinsonism. *Brain*. 2007;130(Pt 1):265-275. doi:10.1093/brain/awl337
44. Linder B, Grozhik AV, Olarerin-George AO, Meydan C, Mason CE, Jaffrey SR. Single-nucleotide-resolution mapping of m^{6}A and m^{6}Am throughout the transcriptome. *Nat Methods*. 2015;12(8):767-772. doi:10.1038/nmeth.3453
45. Dresios J, Aschrafi A, Owens GC, Vanderklish PW, Edelman GM, Mauro VP. Cold stress-induced protein Rbm3 binds 60S ribosomal subunits, alters microRNA levels, and enhances global protein synthesis. *Proc Natl Acad Sci U S a*. 2005;102(6):1865-1870. doi:10.1073/pnas.0409764102
46. Smart F, Aschrafi A, Atkins A, et al. Two isoforms of the cold-inducible mRNA-binding protein RBM3 localize to dendrites

and promote translation. *J Neurochem*. 2007;101(5):1367-1379. doi:10.1111/j.1471-4159.2007.04521.x
47. Zhang Y, Hamada M. Identification of m^{6}A-associated RNA binding proteins using an integrative computational framework. *Front Genet*. 2021;12:625797. doi:10.3389/fgene.2021.625797
48. Peretti D, Bastide A, Radford H, et al. RBM3 mediates structural plasticity and protective effects of cooling in neurodegeneration. *Nature*. 2015;518(7538):236-239. doi:10.1038/nature14142
49. Alarcon CR, Goodarzi H, Lee H, Liu X, Tavazoie S, Tavazoie SF. HNRNPA2B1 is a mediator of m^{6}A-dependent nuclear RNA processing events. *Cell*. 2015;162(6):1299-1308. doi:10.1016/j.cell.2015.08.011
50. Jiang L, Lin W, Zhang C, et al. Interaction of tau with HNRNPA2B1 and N^6-methyladenosine RNA mediates the progression of tauopathy. *Mol Cell*. 2021;81(20):4209-27.e12. doi:10.1016/j.molcel.2021.07.038
51. Liu J, Li K, Cai J, et al. Landscape and regulation of m^{6}A and m^{6}am methylome across human and mouse tissues. *Mol Cell*. 2020;77(2):426-440.e6. doi:10.1016/j.molcel.2019.09.032
52. Fujiwara H, Hasegawa M, Dohmae N, et al. Alpha-synuclein is phosphorylated in synucleinopathy lesions. *Nat Cell Biol*. 2002;4(2):160-164. doi:10.1038/ncb748
53. Tofaris GK, Razzaq A, Ghetti B, Lilley KS, Spillantini MG. Ubiquitination of alpha-synuclein in Lewy bodies is a pathological event not associated with impairment of proteasome function. *J Biol Chem*. 2003;278(45):44405-44411. doi:10.1074/jbc.M308041200
54. Liu SY, Feng Y, Wu JJ, et al. M^6 a facilitates YTHDF-independent phase separation. *J Cell Mol Med*. 2020;24(2):2070-2072. doi:10.1111/jcmm.14847
55. Wang J, Wang L, Diao J, et al. Binding to m^{6}a RNA promotes YTHDF2-mediated phase separation. *Protein Cell*. 2020;11(4):304-307. doi:10.1007/s13238-019-00660-2

SUPPORTING INFORMATION

Additional supporting information can be found online in the Supporting Information section at the end of this article.

How to cite this article: Martinez De La Cruz B, Gell C, Markus R, Macdonald I, Fray R, Knight HM. m^{6}A mRNA methylation in human brain is disrupted in Lewy body disorders. *Neuropathol Appl Neurobiol*. 2023;49(1):e12885. doi:10.1111/nan.12885